Integrated Photonics for Computing, Interconnects and Sensing

Jason Midkiff[1], Ali Rostamian[1], Kyoung Min Yoo[1], Aref Asghari[1], Chao Wang[1], Chenghao Feng[1], Zhoufeng Yin[1], Jiaqi Gu[1], Haixia Mei[1], Ching-Wen Chang[1], James Fang[2], Alan Huang[2], Jong-Dug Shin[2], Xiaochuan Xu[2], Michael Bukshtab[2], David Pan[1], and Ray T. Chen[1,2]

[1]Microelectronics Research Center
The University of Texas, Austin
10100 Burnet Rd., Building 160
Austin, TX 78758

[2]Omega Optics Suite 200
8500 Shoal Creek Blvd.
Austin, TX 78757
chenrt@austin.utexas.edu

Integrated photonics is poised to revolutionize inter- and intra-data center communications since internet traffic continues to increase exponentially, making it difficult and costly for existing switching and interconnects in data centers to cope with the fast-growing bandwidth requirement. Integrated photonics is able to contribute to data centers in terms of lower cost, higher bandwidth, and lower power consumption. As many fundamental components including the power-efficient modulators mature, integrated photonics is believed to have reached the tipping point with a surging global market. Besides the optical interconnects, Integrated photonics also shows promise in abundant applications, ranging from high-performance optical computing and Lidar for autonomous cars to biomedical sensing and even aerospace applications.
In this invited paper, an overview of the integrated photonics as well as a potential trend for the next decade will be provided. First, the recent development of optical components including passive and active modules as well as optical circuits in silicon and III-V compound based integrated photonic devices will be presented. Figure 1 shows the first InP based optical phased array operating at 4.6-micron wavelength with a waveguide spacing of 2.5λ, we steer the beam to the maximum uninfringed field-of-view at ±11.5°[1].

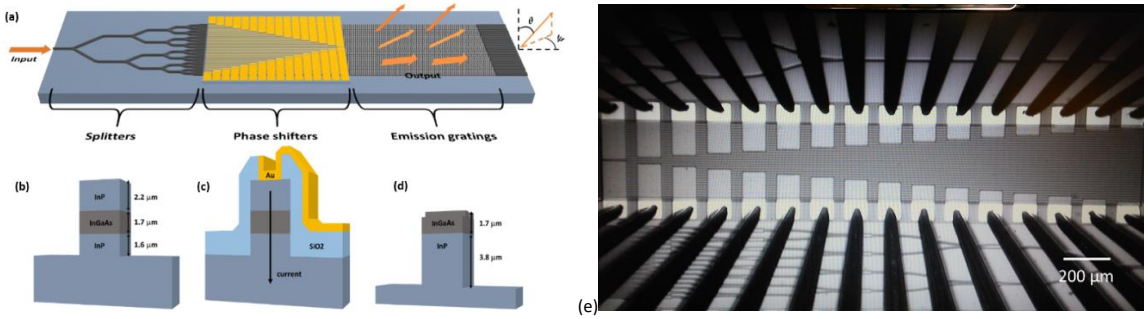

Fig. 1. Schematic illustrations of the OPA device (not to scale). (a) Entire layout with input and output light indicated. Also shown, ψ the azimuthal angle, and θ the elevation angle. (b), (c), and (d) Cross-sections of the ridge waveguide structure in the splitter, phase shifter, and emission grating regions, respectively. Also indicated in (c) is the current flow for resistive heating of the phase shifter. And (e)) Microscope photo of 32 phase shifters contacted by the probes.

Second, as Moore's law has been approaching the physical limitation, photonics-based high-performance computing is envisioned as a potential answer to the continuation of Moore's law[2]. We propose and experimentally demonstrate a new photonics-assisted full adder which is capable of operating at a higher frequency than electrical counterparts while consuming less power[3]. This paves the way to the future integrated high-speed and power-efficient optical computing.

Finally, sensing related applications will also be addressed in the presentation. Both spectroscopy sensing for various analytes including chemical warfare agents (CWA) and greenhouse gases will be covered. An open platform for biomarker detection on a silicon photonic chip is also developed with TRL 6 (Technology readiness level). The biomarkers we reported so far including breast cancer biomarker, lung cancer biomarker, pancreatic cancer biomarkers, three Antibiotic drugs and heavy metal attached biomarkers. One of the guided meta-surface is shown in Figure 2 where unprecedented sensitivity to femto mole level without sacrificing the specificity [4]. The surface sensitivity S_s can be defined as below,

$$S_s = \frac{\Delta\lambda}{\Delta t} = \frac{\lambda}{n_g}\left(\frac{\partial n_{eff}}{\partial t}\right), \qquad (1)$$

where $\Delta\lambda$ is the resonance wavelength shift, Δt is the change of surface layer thickness, ∂n_{eff} the effective refractive index of the waveguide mode, and n_g is the group index. According to H. Yan *et al.* simulation and experimental results, the large mode overlapping factor provides the 4-6 times higher $\frac{\partial n_{eff}}{\partial t}$ in the SGM microring resonator than the regular strip microring resonator [5]. That means the SGM microring resonator has superior surface sensitivity and better sensing capability over regular strip microring resonator. Fig. S3 shows experimental surface sensitivity comparison of the SGM microring resonator and the regular strip microring resonator.

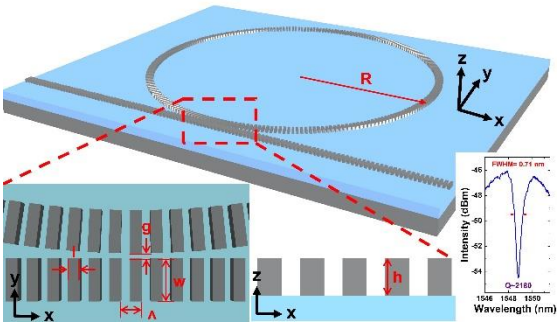

Figure 2 The schematic of metasurface waveguide microring resonator, where R is the diameter of the microring, Λ is the subwavelength grating period, h is the thickness of waveguide core, w is the width of waveguide core, l is the length of silicon pillar, and g is the gap between microring and bus waveguide. The right-bottom insert shows transmission spectrum of the fabricated microring.

A fully automated portable silicon-based optical biosensing system has been successfully demonstrated. It is essentially based on a subwavelength grating metamaterial microring resonator structure down to the nanoscales of 50 nm. When adequately designed, the subwavelength grating metamaterial microring sensor demonstrates unprecedented sensitivity on a myriad of biomarkers. The graphic user interface written in MATLAB for system manipulation is designed with ease of use in mind. The real-time relative resonance peak shifts observed in streptavidin detection for regular SWG microring resonators also proves excellent system performance. The same open biosensing platform can also be employed for COVID19 detection with the integration of the microfluidic channel containing the saliva-based COVID-19. Label-free microarrays are particularly exciting because it simplifies biochemistry significantly when probe-target binding conjugations can be studied without steric hindrance associated with fluorescent or radioactive tags. In Fig. 3, we depict our photonic crystal microarray approach using photonic crystals (PCs) and show that our microarray has the highest sensitivity to small changes in concentration. Our recent work[6] summarizes sensitivities and detection limits demonstrated in our system compared to other label-free methods, including surface plasmon resonance (SPR), optofluidic ring resonators (OFRR), ring resonator (RR) Pedestal SMGMR, and photonic crystal (PC) devices, as function of sensing area. Sensitivities of PC microcavity structures demonstrated at Omega Optics (OO) and University of Texas (UT), Austin is indicated by UT/OO. Further result will be presented in the conference.

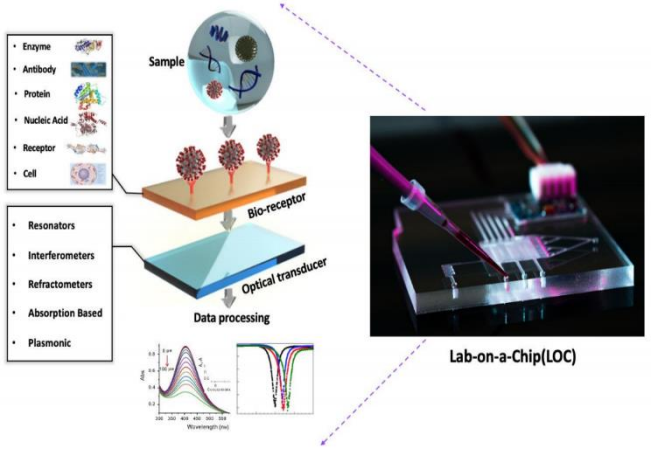

Figure 3 Schematic working principle of a lab-on-a-chip (LOC) optical biosensor.

References

1.Jason Midkiff, et al., Optica, accepted for publication Oct. 5, 2020.
2.Ray Chen, et al., Proceedings of IEEE, Vol.88, pp.780-793(2000)
3.Zhoufeng Ying, et al.,Nature Communication 11, 2154 (2020).
4. Varun Soni, et al.,IEEE Transactions on Biomedical Engineering, accepted for publication, 2020.
5. H.Yan *et al.*, *Opt. Express*, vol. 24, no. 26, p. 29724, 2016, doi: 10.1364/oe.24.029724.
6. Aref Asghari[1], et al., Invited Paper to Applied Physics Review (Under Review)